THE JOURNAL OF PHYSICAL CHEMISTRY C

Article

pubs.acs.org/JPCC

Coherent and Diffusive Time Scales for Exciton Dissociation in Bulk Heterojunction Photovoltaic Cells

K. Birgitta Whaley,*[,†] Aleksey A. Kocherzhenko,[†] and Abraham Nitzan[‡]

[†]Department of Chemistry, University of California, Berkeley, California 94720, United States

[‡]School of Chemistry, Tel Aviv University, Tel Aviv, 69978, Israel

Supporting Information

ABSTRACT: We study the dynamics of charge separation in bulk heterojunction organic photovoltaic systems in light of recent experimental observations that this process is characterized by multiple time scales in the range of 10 fs to 100 ps. Coherent evolution of the excitonic state has been suggested to dominate the early stages of the charge separation process and diffusion of localized excitons to be dominant at longer times. Both of these processes obviously depend on the system morphology, in particular on the grain sizes of the donor and acceptor phases. Here we analyze these mechanisms and their characteristic time scales, aiming to verify the consistency of the proposed mechanisms with the experimentally observed time scales of charge separation. We suggest that the coherent mechanism that dominates the early stage of charge separation involves delocalized excitons. These excitons are formed by optical excitation of clusters of strongly interacting donor sites, and the charge separation rate is determined by the probability that such sites lie at the donor−acceptor interface. The (relatively) slow diffusive rate is estimated from the mean first passage time for a diffusing exciton to reach the donor grain surface. Our estimates, based on available exciton diffusion rates and morphology data, are consistent with experimental observations.

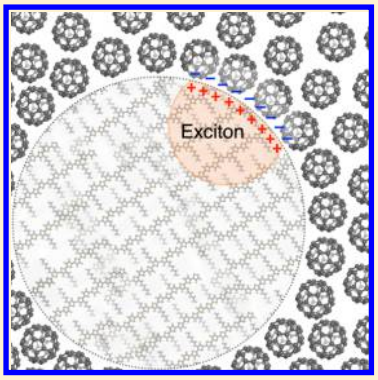

1. INTRODUCTION

Energy conversion in photovoltaic cells results from a succession of processes, each of which can affect the overall performance of the device. In bulk heterojunction organic photovoltaic (BHJ-OPV) cells these processes (some of which may be coincidental) are (a) optical absorption to form excitons, (b) exciton migration to the donor (D)−acceptor (A) interface, (c) short-range electron transfer at the DA interface to form interfacial charge transfer exciton, (d) exciton dissociation and charge separation, (e) charge stabilization (polaron formation) by environmental reorganization, (f) geminate and nongeminate charge recombination, (g) electron and hole motion in their host phases, and (h) charge collection at the electrodes. Understanding the interplay between these processes is at the core of our attempts to enhance solar cell performance, as measured by the internal and the external energy conversion efficiencies. Understanding the underlying mechanisms of the individual processes is an important prerequisite to this end, in addition to being of fundamental interest.

The present work deals with the early stages of the above sequence of processes—exciton formation and migration to the donor−acceptor interface. It is motivated by recent observations that appear to contradict the standard view that following generation, excitons propagate to the DA interface by a diffusion process. We summarize the key experimental observations as follows:

(a) The diffusion constant D of singlet excitons in organic crystals is of the order of 10^{-3}−10^{-5} cm^2 s^{-1}.[1,2] Obviously, the time it takes to reach a DA interface depends on the sample morphology. Typical grain-sizes observed in TEM images in the more finely distributed samples are of the order $R \approx 10$−20 nm.[3−6] For $D = 10^{-3}$ cm^2 s^{-1}, the time to reach the boundary by classical diffusive motion starting from the center of such a region is of the order $R^2/6D \approx 150$ ps.

(b) In contrast to such estimates of exciton diffusion times of $\sim 10^2$ ps, a number of recent observations indicate that a substantial part of the total charge generation occurs on a much faster time scale of 20−200 fs following generation of the excitons by an optical pulse. For example, Jailaubekov et al.[7] have studied a system comprising copper phthalocyanine (CuPc)/fullerene bilayers. They used time-resolved second harmonic generation to monitor the development of the electric field across the DA interface (a signature of charge transfer at this interface) and time-resolved 2-photon photoemission to follow the populations of excitonic states, both on the femtosecond time scale. They observe charge transfer (CT) excitons forming at the interface on time scales of ∼100 fs for excitation frequency 1.85−2.00 eV. This time is frequency dependent: for excitation at 1.55 eV the CT excitons form at 0 ± 20 fs, consistent with direct optical pumping into this state. Using transient (pump−probe) absorption (TA) spectroscopy, Kaake et al.[8] have studied the dynamics of photoinduced charge separation in several organic nanostructured BHJ systems and

Received: August 24, 2014
Revised: October 15, 2014
Published: October 23, 2014

   dx.doi.org/10.1021/jp508561z | J. Phys. Chem. C 2014, 118, 27235−27244

found that the majority of charge carriers are generated within the experimental time resolution of <100 fs. Interestingly, however, about one third of the charge carriers are nevertheless formed on a much longer time scale, ∼50 ps, which is close to the order estimated for an exciton diffusion process. Charge separation taking place on fast (<100 fs) and slow (∼10 ps) time scales was reported by Guo and co-workers[9] in TA spectroscopic studies of a blend film comprising poly(3-hexylthiophene) (P3HT) and [6,6]-phenyl-C71-butyric acid methyl ester (PCBM). Similar observations were made by Marsh et al.,[10] who have further studied the effect of annealing on the exciton decay and charge separation dynamics in this system (see below). Again using TA spectroscopy, Grancini and co-workers[11] report fast (∼100 fs) interfacial generation of both charge transfer excitons and free polarons in the poly[2,6-(4,4-bis(2-ethylhexyl)-4*H*-cyclopenta[2,1-*b*;3,4-*b*′]-dithiophene)-*alt*-4,7-(2,1,3-benzothiadiazole) (PCPDTBT)/$PC_{60}BM$ BHJ system. These observations depend on the photoexcitation energy, but there is no clear trend. For example, Grancini and co-workers[11] suggest that there should be a correlation between higher excitation energy and short formation time, but the authors of ref 7 see an opposite correlation.

(c) In an exciton diffusion based model, we would normally expect better cell performance to correlate with larger exciton diffusion coefficients. This correlation is not clearly observed. Mikhnenko et al.[1] report a decrease in the measured exciton diffusion length in annealed polycrystalline samples of 2,5-dihexyl-3,6-bis[4-(2,20-bithiophene-5-yl)phenyl]pyrrolo[3,4-*c*]-pyrrole-1,4-dione (C6PT2-DPP)/PCBM, contrary to expectations based on observations of improved performance of solar cells based on this material (see, however, a recent report of reduced performance upon annealing in another system[12]). While interpretation of this measurement is complicated by possible effects of changes in the exciton lifetime and domain boundaries upon annealing, this observation is consistent with measurements of a slower long time (diffusion controlled) component of the charge separation dynamics observed in annealed P3HT/PCBM blends compared to dynamics in the corresponding pristine system.[10] These measurements suggest that exciton diffusion is not necessarily the primary factor in the overall charge separation process in OPV cells. Note, however, that in other systems, such as poly(*p*-phenylenevinylene) (PPV)/fullerene heterostructures,[13] where the amount of disorder is controlled by chemical modification of the side chains in the PPV system, the expected increase in exciton diffusion coefficient upon decreasing disorder is observed. More results on the interplay between morphology and cell performance in BHJ-OPV systems are provided in a recent review.[14]

The authors of refs 7−11 and 15 (see also ref 16) suggest that the observed fast charge separation is associated with the delocalized nature of the excitons formed in the absorber phase.[17] Indeed, long exciton coherence lengths have been demonstrated in ordered (low temperature) single conjugated polymer chains.[18] A long known distinction between two types of coherences in many-chromophore systems was recently emphasized by Mukamel.[19] One is the spatial coherence associated with exciton delocalization and the other is coherence between eigenstates. The experiment of ref 18 demonstrates both. It is intuitively clear (see also refs 19 and 20) that if (a) the exciton is strongly delocalized over the entire extent of an excited aggregate and (b) there is a mechanism causing exciton dissociation at the aggregate surface, then exciton dissociation will follow its optical generation on a time scale that is unrelated to the exciton diffusion properties and that can be much faster than the exciton diffusion time. This situation will hold whenever the initial state is an excitonic eigenstate rather than a localized optical excitation, which is the case when the coherence length of the incident light is at least as large as the length scale of exciton delocalization. This picture can be generalized to situations where the delocalized exciton is smaller than, but of the same order as, the size of the excited aggregate, or when the exciton delocalization size decreases with time. In particular, we expect that the relative contributions of the fast and slow components of the charge separation process will be dependent on the ratio of grain size to exciton size, with an increase in grain size making the slow component more prominent. While the morphology of the BHJ systems described above is too complex to allow systematic measurements of this effect, such behavior was indeed recently observed[21] in measurements of exciton survival in a film of zinc phthalocyanine (ZnPc) deposited on gold, where excitons are photoexcited in the ZnPc layer and decay by electron transfer to the metal substrate.

Supporting, albeit indirect, evidence for ultrafast charge separation following photoexcitation of DA composites can also be found in time-resolved observations of singlet exciton fission. Using time-resolved 2-photon photoemission (TR-2PPE) spectroscopy, Zhu and co-workers have recently demonstrated that the process by which a singlet exciton can split into two triplet excitons (a potentially useful pathway for increasing the charge generation rate, although not necessarily the generated power, of a photovoltaic cell) involves a "multiexciton" state that appears to be a coherent superposition of the singlet and a two-triplet state.[22,23] Congreve et al. have indeed shown that in a pentacene/C_{60} based solar cell (with an exciton blocking layer of regioregular poly(3-hexylthiophene) (P3HT) placed between the pentacene and the anode), the external quantum efficiency can exceed 100% and the internal quantum efficiency can exceed 150%.[24] From the magnetic field dependence of the photocurrent they deduce a triplet yield of 200%. These results depend, however, on the thickness d of the pentacene layer, with the yield decreasing significantly for $d < 5$ nm.[25] This reduction in the triplet yield for small d values indicates that the S → 2T process is suppressed by some form of singlet annihilation at the DA interface. Given that the S → 2T transition is itself a sub-100 fs process,[22,23,26] the corresponding singlet annihilation must take place on the same time scale. This strongly suggests that the competing singlet relaxation mechanism in singlet exciton fission could be an ultrafast charge separation process at the DA interface and is consistent with the suggestion[27] that the initially formed S1 exciton in tetracene is delocalized over 10^3−10^4 sites. The interesting question whether the triplet, or indeed the multiexciton S-(2T) state, is formed coincidentally with the singlet state during the optical excitation, or whether the singlet is a precursor of these states, is analogous to the issue of the nature (delocalized or localized) of the photogenerated exciton discussed above. In fact, both scenarios can occur: since both the S and the (2T) states have singlet character, either of these states or their coherent linear combination may be produced during the photoexcitation pulse, as indicated by the simultaneous appearance of the 2PPE signals associated with the singlet and with the triplet in the experiments of refs 22 and 23. However, if the S−(2T) coupling is not too large, part of

the triplet signal will appear subsequent to the singlet, as seen in ref 26. It is this later signal that can be suppressed by the competing exciton relaxation at the DA interface.

The above discussion indicates that the dynamics of charge separation in bulk heterojunction photovoltaic cells is a multi-time scale process, with a fast ≤100 fs component (the actual times are morphology dependent) that is dominated by the initially excited delocalized excitons, and a slower, diffusion-controlled component. The latter reflects the contribution from initially localized excitons, as well as contributions from initially delocalized excitons that become localized on a time scale ≤100 fs due to dephasing and energy relaxation induced by the underlying nuclear motion.[28,29] It should be kept in mind that such delocalization and diffusion-controlled dynamics are interdependent: the exciton diffusion coefficient itself depends on the exciton delocalization length,[31] and is therefore time dependent at early times as localization proceeds.[28] The photoexcitation process can form excitons with finite delocalization lengths (that can depend on the excitation frequency[32]) near the DA interface or further away from it. The observed early time charge separation can then be rationalized as reflecting the dissociation of excitons that overlap the interface immediately after excitation, as well as those that form within the interior of the chromophore aggregate but are able to reach the interface by rapid coherent transport ($t \lesssim 200$ fs). On the other hand, it is reasonable to assume that the observed long time component (~50 ps)[8] of the charge separation process reflects the standard diffusion of localized excitons, i.e., true Frenkel excitons that are localized on single sites. Here the long time exciton localization length is determined by the intersite energy transfer coupling strength and the dynamic (exciton−phonon interaction) and static disorder, and is typically of order 1−10 chromophore sites.[28,33,34]

To better understand the multiscale excitonic energy transfer in BHJ−OPV systems it is also useful to compare them with the natural photosynthetic systems, where high internal quantum efficiencies are found and for which time-resolved spectroscopic measurements of energy transfer have revealed considerable insight into the nature and mechanism of excitonic energy transport. In contrast to bulk heterojunction systems, the antenna "light harvesting" complexes of photosynthetic systems are highly organized and the energy flow is generally directed from peripheral structures where the light is absorbed, toward relatively small and well-defined reaction centers in which the charge separation occurs. Excitonic transport is understood to involve a complex interplay between coherent and incoherent dynamics, which is very sensitive to the dephasing and dissipative interactions with the protein scaffold. A brief overview of these issues is given in Section 2 below.

In the present paper we examine the above picture of multi-time scale charge separation in a more detailed, yet still qualitative way, aiming to verify its consistency with available data on chromophore aggregate size, exciton interfacial dissociation dynamics, exciton localization length, and exciton diffusion. In Section 2 we introduce relevant concepts and language and consider excitonic energy transfer in a broader scope by giving a brief overview of excitonic delocalization and coherence effects in molecular arrays, conjugated polymers, and biological light harvesting systems, while commenting on similarities and difference to the analogous processes in organic photovoltaic systems. In Section 3 we analyze the fast (~100 fs) dynamics using a model that assumes a delocalized initial exciton state to derive a relationship between the observed rate, the aggregate size, and the exciton delocalization length. Section 4 provides a similar analysis for the relatively slow (~50 ps) time scale that is presumed to be diffusion controlled. The combined analysis provides a consistent picture of the charge separation dynamics following a short pulse excitation, for several BHJ−OPV systems. Section 5 summarizes and concludes.

2. EXCITON DELOCALIZATION AND COHERENT TRANSPORT

Excitonic states produced by photoexcitation of molecular aggregates exhibit a wide range of spatial and dynamic characteristics. In idealized molecular arrays composed of identical repeat units coupled by dipole−dipole interactions, without static or dynamic disorder, band-like excitonic states that are delocalized over the entire array are predicted.[35] The delocalized band states show characteristic superradiance, shifts of absorption spectra relative to the monomer species that depend on the geometry and intermolecular interactions and characteristic nonlinear spectroscopic properties.[36−38] In practice, the extent of delocalization is limited by energetic and spatial disorder of the molecular components, by coupling to phonon modes, and by dynamical disorder deriving from the detailed nuclear dynamics of the environment. Nevertheless, many spectroscopic features of molecular excitonic systems may be understood in terms of the properties of idealized molecular arrays. Thus, the well-known H- and J-aggregates show characteristic blue and red spectral shifts in absorption, respectively,[39] reflecting repulsive and attractive intermolecular interactions. In addition, due to symmetry constraints on multiple exciton states, the energy differences between one- and two-exciton bands are larger than the energy difference between ground and one-exciton states, by an amount that depends on the size of the delocalized state, allowing the delocalization length to be estimated from nonlinear spectroscopies such as pump−probe spectroscopy[40] or from excess polarizabilities.[41] Experimental studies on J-aggregates formed from cyanine dyes have shown coherence lengths on the order of 60−100 molecules.[39]

Photoexcitations of conjugated polymers, both pure and in blends, share these basic features but are strongly influenced by coupling of the π-excitations to phonon modes of the polymer backbone, giving rise to structural relaxation[42] and self-localization, as well as by quasi-one-dimensional disorder-induced localization.[43] Exciton delocalization in these systems is consequently restricted and strongly dependent on the detailed conformational structure and packing morphology. A common model is to assume delocalization over variable numbers of π-conjugated bonds lying within "chromophore segments" that are only weakly coupled, reflecting the disruption of the π-conjugated electronic system by torsions, conformational changes, and energetic disorder. The delocalization can nevertheless be extended over multiple segments: theoretical studies sampling conformations of poly(phenylenevinylene) (PPV) chains with vibronic couplings show excitonic eigenstates broadly distributed over 2−6 segments of up to 25 monomeric units.[34] Notably, this distribution of excitonic eigenstates shows no significant correlation with the absorption spectrum, but the presence of delocalized eigenstates results in faster fluorescence anisotropy decay, consistent with more efficient exciton migration along the polymer chain in a Pauli master equation description of transitions between excitonic eigenstates.[44−46]

dx.doi.org/10.1021/jp508561z | J. Phys. Chem. C 2014, 118, 27235−27244

Excitonic delocalization is also well established in photosynthetic light harvesting complexes, antenna structures whose role is to absorb light, convert it to electronic excitation energy, and transport this to the photosynthetic reaction center. These are typically pigment−protein complexes with high concentrations of chromophores such as chlorophyll, ensuring high proximity and relatively strong interchromophore interactions.[47] Chromophore proximity and strong couplings result in exciton delocalization. While not as large as in J-aggregates, such delocalization is quite common in light harvesting complexes. Thus, the B850 ring of LHII in purple bacteria shows delocalization over 2−9 of its 18 chlorophylls[48,49] while cryptophytes[50] and even peripheral light harvesting structures such as the FMO complex show exciton delocalization over pairs of chlorophyll molecules.[51] Enhancement of electronic energy transport by transitions between delocalized excitonic states has been widely studied for light harvesting with a multichromophoric Forster rate theory[52] and extensions of this.[53−57] For example, energy transport enhancement due to delocalization over the B850 ring is predicted to enhance transport between the B800 and B850 rings of LHII in purple bacteria by a factor of 5.[58,59] The interaction between electronic and vibrational degrees of freedom is critical for understanding the origin of such excitonic coherence. Theoretical analysis has shown that these coherences may be generated from initialization in a single exciton eigenstate,[30] underscoring the complex role of the vibrational environment of the protein and its coupling to the electronic excitations. More intriguingly, recent theoretical studies have indicated that energy transport in light harvesting complexes is optimal with respect to all known parameters.[61] These naturally evolved pigment−protein structures thus appear to be exquisitely tuned with regard to structure, electron-vibration couplings and all spectral properties, to ensure optimal delivery of excitonic energy from the antenna to the reaction center for charge separation.

Despite the complex nature of such combined coherent (unitary) and incoherent (dissipative, dephasing) processes which, as mentioned above, can be sensitive to details of the exciton−vibration coupling, the features most relevant to the present work may be qualitatively represented within a tight-binding model of quantum transport subject to classical dephasing noise, i.e, a Haken Strobl model.[31,62] In the absence of energetic disorder, the excitonic dynamics are well understood[63] and show a transition from short time coherent motion characterized by ballistic transport ($\langle x^2\rangle \propto t^2$) to incoherent diffusive transport ($\langle x^2\rangle \propto t$) at long times. In the presence of disorder, quantified by the variance σ of nearest neighbor exciton energy differences, the dynamics are always diffusive. Nevertheless, while the predominant contribution is hopping between neighboring sites, for small dephasing $\Gamma \ll J$, where Γ is the dephasing rate and J is the intersite energy transfer coupling, there is an additional contribution from delocalized excitons, described approximately by $D = \Gamma\xi^2$, where ξ is a measure of the exciton delocalization.[31] For weak noise, the dephasing time Γ^{-1} is long compared to the time for coherent (ballistic) motion between sites J^{-1}, while for strong noise it is much shorter and coherence is maintained only during hopping between individual sites but not between hopping events. Consideration of this simple one-dimensional model also suggests that when the intersite energy transfer coupling is strong, and dephasing and dissipation weak enough to maintain coherent energy propagation over some length scale, an initial excitation will be delocalized over this same length scale, provided that the exciting light is characterized by a similar or larger coherence length. Such simple 1-dimensional models are particularly useful when well-defined spatial pathways for energy transfer exist, as in the FMO complex;[51,62] however, the qualitative features of such models are expected to persist in higher dimensions and we shall make use of this general expectation in our analysis of exciton dissociation dynamics below.

Such dephasing models are widely used to discuss the mechanisms of vibrationally assisted coherent transport in light harvesting systems[64,65] and are now also being used to analyze the role of vibration−exciton coupling in ultrafast charge separation.[66]

3. DISSOCIATION OF DELOCALIZED EXCITONS

As outlined in the Introduction, there is a growing awareness that a substantial fraction of charge generation in BHJ−OPV cells does not involve exciton diffusion to a donor−acceptor interface, but instead involves delocalized excitons. This conclusion follows from observations of charge separation on the time scale of $\lesssim$100 fs in a number of BHJ systems.[7,8,11,16,28,67,68] Similar observations are made with respect to exciton fission that appears to take place on similar time scales.[23,69] However, the issue is more intriguing for the exciton dissociation process, where the excitation has to reach a local donor−acceptor interface. In addition, a recent observation indicates that a significant role is played by delocalization in the acceptor phase,[70] leading to a large spatial separation between electrons and holes on a time scale of ∼50 fs, followed by a fast (<300 fs) polaronic stabilization of the separated charges.[71]

The implication of exciton delocalization for exciton dissociation and charge separation may be usefully considered in the context of coherent vs incoherent transport, as in the light harvesting systems discussed in Section 2. As indicated there, both the coherent or incoherent nature of this transport and the time scale on which it is coherent are determined by the relative magnitudes of the intermolecular excitonic coupling J and the inverse thermal relaxation and dephasing times. As long as the delocalization is maintained, exciton dissociation will be determined not by the time it takes for a localized exciton to reach the donor−acceptor interface but by the probability to find some component of a delocalized exciton at the interface. This is illustrated schematically in Figure 1.

The dynamics of exciton dissociation, even on this short time scale, involves a host of competing processes. A minimal model

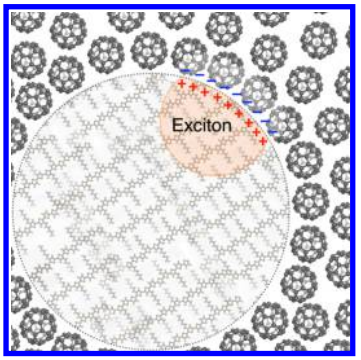

Figure 1. Schematic of a delocalized exciton in a polymeric donor grain (e.g., P3HT), surrounded by acceptor (fullerene), with charge separation of the exciton occurring at the donor−acceptor interface.

for its description should include two grains, donor and acceptor, with N_D and N_A sites, respectively, and with a given interface between them at which exciton dissociation can take place. A convenient basis in the site representation includes exciton states, $|n_D\rangle$; $n_D = 1, ..., N_D$ on the donor and electron−hole states $|n_D n_A\rangle$, $n_D = 1, ..., N_D$; $n_A = 1, ..., N_A$, where N_D, N_A correspond to the sizes of the donor and acceptor species, respectively. Intersite coupling induces excitation hopping in the donor environment and electron and hole hoping in their respective acceptor and donor environments. Additional coupling between those $|n_D\rangle$ and $|n_D n_A\rangle$ states that are located at the donor−acceptor interface is responsible for the exciton-dissociation process.[72] Coupling to the underlying nuclear environment leads to exciton localization in the donor phase and electron and hole localization (polaron formation) in their respective environments.

A full model of the exciton dissociation should account for the short time behavior of the charge separation process, including the time evolution of interface charging and the distance between the electron and hole charge densities, as well as their dependence on the donor and acceptor grain sizes, coherence lengths, intersite coupling, and localization rates. In general this time evolution will not be simple. First, it may be convoluted with the photoexcitation process. Second, the charge separation rate will evolve with the changing distribution of site excitations and intersite coherences in the donor phase. In what follows we take a much simplified route and provide a rough estimate of the charge separation rate that is based on the assumption that this rate is given by the probability to find an excited donor on a given interfacial site, multiplied by the rate of the $ex \rightarrow eh$ process (ex denotes exciton, eh denotes electron−hole pair, with hole in the donor and electron in the acceptor) starting from this site. These probabilities and rates are estimated below.

Consider first the rate at which electron transfer from an excited donor molecule into the acceptor phase takes place at the donor−acceptor interface. The conventional picture of this process is a Marcus-type transition where irreversibility is driven by nuclear reorganization in the donor and/or acceptor phases (see, e.g. Chapter 16 in ref 73). If the donor−acceptor pair is optimized for efficient charge separation, the corresponding Marcus process will be nearly activationless. In BHJ−OPV systems this is achieved by tailoring the LUMO−LUMO gap between the donor (D) and acceptor (A) molecules to match the exciton binding energy so that the excited state on an interfacial donor molecule lies within the band of charge separated states $|D^+A^-\rangle$. The semiclassical Marcus nonadiabatic rate in this limit takes the form $k = (1/\hbar)[\pi/E_R k_B T]^{1/2}|V_{DA}|^2$, where V_{DA} is the electron transfer coupling and E_R is the reorganization energy. Using typical values of $V_{DA} = 0.1$ eV (for molecules in contact) and $E_R = 0.1$ eV yields a value $k \approx 3 \times 10^{-14}$ s^{-1} at room temperature. Such ultrafast electron transfer rates that exceed the speed of solvent motion as well as the experimental time resolution are well-known[74,75] and electron injection rates of such order have also been reported.[76]

Based on the observation[70] that electron−hole separation in BHJ−OPV systems can reach a distance of ∼4 nm on a time scale of ∼50 fs, another scenario for the exciton dissociation can be constructed, in which the charge separation is driven not by nuclear reorganization but by interband dynamics. In this picture the charge transfer results from overlap between the exciton band in the donor grain and bands of electron−hole pair states in the donor and acceptor grains. For example, a rough estimate of the injection rate from an excited interfacial donor molecule to a "final" manifold of electronic states composed of a hole in the donor molecule combined with an excess electron moving in the acceptor LUMO band is obtained from (see, e.g., Chapter 9 in ref 73)

$$k_{D\rightarrow A} \approx \frac{|V_{DA}|^2}{(E_D - E_A)^2 + (\Gamma_A/2)^2}\frac{\Gamma_A}{\hbar} \approx \frac{4|V_{DA}|^2}{\hbar\Gamma_A} \quad (1)$$

where $E_D - E_A$ is the electronic energy difference between the exciton state and the electron−hole (e−h) band center (in single electron language, the difference between the LUMO−LUMO gap and the exciton binding energy), while Γ_A is the width of the latter (e−h) band. With typical orders of magnitude $|V_{DA}| \leq \Gamma_A \approx 0.1$ eV, this again implies injection rates in the ∼5 fs time scale.

Now consider the probability that an interfacial donor site is excited following pulse excitation of the donor grain. For the sake of a rough estimate assume that the donor grain is a spherical particle of radius R_D and that the coherence length of an exciton is R_x. Then an optical excitation of the bulk donor forms, on average, a spherical cluster of strongly interacting excited sites of radius R_x (see Figure 2). We further assume that

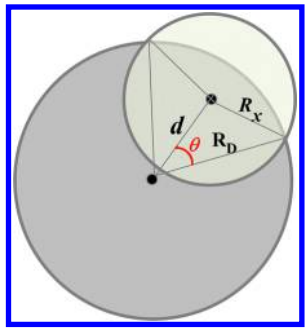

Figure 2. Spherical donor grain—spherical exciton model used for estimating the probability P_x that the exciton overlaps with the donor−acceptor interface at the donor grain boundary.

$R_x \leq R_D$ and estimate the number of excited interfacial sites. A rough estimate (see the Supporting Information) of the probability P_x that the coherent exciton on the donor grain overlaps the interfacial region (and therefore is subjected to the fast charge separation process discussed above) yields

$$P_x = \frac{3a}{R_D}\left(1 - \frac{a}{R_D}\right)\frac{1}{\left(1 + \frac{R_x}{R_D}\right)^3} \quad (2)$$

where a is the size of a molecular site. For $R_x/R_D \approx 1/3$ and $a/R_D \approx 1/5$, we obtain $P_x \approx 0.2$. Combining this with the estimate of $\tau_{DA} \approx (5\text{ fs})^{-1}$ from eq 1 for the rate of charge separation across the donor−acceptor interface results in an exciton dissociation rate of $\tau^{-1} = P_x\tau_{DA}^{-1} = (60\text{ fs})^{-1}$ $\tau^{-1} = P_x\tau_{DA}^{-1} \approx (25\text{ fs})^{-1}$ and hence in a time scale for exciton dissociation of $\tau \approx 25$ fs. It should be emphasized that this exciton lifetime represents a rate process with rate $\sim\tau^{-1}$ only in the limit where the coupling between the sites comprising the exciton is strong enough relative to dephasing, environment-induced dissipation and dissociation to maintain the coherent nature of the exciton during its dissociation (see the discussion in Section 2).

dx.doi.org/10.1021/jp508561z | J. Phys. Chem. C 2014, 118, 27235−27244

4. DIFFUSION-CONTROLLED EXCITON DISSOCIATION

On longer time scales, $t > 1$ ps, exciton−phonon interaction leads to loss of coherence as well as to exciton localization, and further charge separation at the grain interface is controlled by successive incoherent (Förster) energy transfer events whose macroscopic expression is exciton diffusion. We now estimate the rate of the resulting diffusion-controlled exciton dissociation at the donor−acceptor interface. It should be noted that as the process of interfacial exciton dissociation proceeds, the probability that a donor molecule is excited will become smaller at the interface than in the bulk, so the dynamics will not be described by a single rate but will in general be multiexponential: the diffusion-controlled rate we estimate below constitutes an upper bound on the actual rate. We may reasonably assume that the radius R_D of the spherical donor grains is small enough to neglect changes in the light intensity due to absorption and that the exciting light has coherence length larger than the grain dimension. In this case the illumination produces a uniform distribution of excitons within the donor grain, $\rho(r,0) = \rho_0$, where $r < R_D$ is the distance from the center of the spherical grain. We also assume that excitons reaching the grain boundary immediately and irreversibly dissociate into free charges. Under this assumption the exciton dissociation process is subject to the absorbing boundary condition

$$\rho(R_D, t) \equiv 0 \tag{3}$$

and its rate can then be estimated by the inverse mean first passage time to reach the interface.

As argued above, such an estimate constitutes an upper bound to the time average rate. Obviously, in reality the probability to dissociate at the interface can also be less than unity, which also implies that the rate calculated below is an upper bound. On the other hand, the requirement that charge dissociation involves only excited interfacial donor molecules may be too stringent and dissociation may already occur at some distance from the interface, which will have the opposite effect. Taken together, it is therefore reasonable to use the mean first passage time calculated within the spherical grain model as a rough measure of the diffusion-controlled exciton dissociation rate.

The instantaneous exciton distribution within the donor grain, $\rho(r,t)$, can now be found by solving the diffusion equation

$$\rho(r, t) = D\nabla^2\rho(r, t) \tag{4}$$

where D is the exciton diffusion coefficient, and the Dirichlet-type boundary condition is given by eq 3. For a radially uniform and azimuthally symmetric initial distribution this problem has an analytical solution in the form of the series[77]

$$\rho(r, t) = 2\rho(r, 0) \sum_{n=1}^{\infty} (-1)^{n+1} \exp\left(-\frac{Dn^2\pi^2 t}{R_D}\right) \frac{\sin(n\pi r/R_D)}{n\pi r/R_D} \tag{5}$$

If the excitons only disappear from a donor grain by means of dissociation at the donor−acceptor interface, the probability of an exciton remaining in a donor grain at time t (the survival probability) can be calculated as

$$P_s(t) = \frac{1}{\rho_0 V} \iiint_V \rho(\mathbf{r}, t)\, \mathrm{d}V = \frac{1}{\rho_0 V} \int_0^{R_D} 4\pi r^2 \rho(r, t)\mathrm{d}r \tag{6}$$

where $V = 4\pi R_D^3/3$ is the total volume of the spherical donor grain. The probability that an exciton has reached the boundary of the donor grain (the first passage probability) at or before time t is then $P_{fp}(t) = 1 - P_s(t)$, and the corresponding probability density is $p_{fp}(t) = -(\partial/\partial t)P_s(t)$. The first moment of the first passage time distribution, the mean first passage time,

$$\tau_{mfp} = \int_0^{\infty} t p_{fp}(t) \quad \mathrm{d}t \tag{7}$$

can be taken as the characteristic time scale of exciton diffusion to the donor−acceptor interface.

Equations 5 and 6 can be evaluated numerically (see the Supporting Information). The survival probabilities calculated according to these equations for typical grain sizes and diffusion coefficient values are plotted in Figure 3. The mean first passage times for the values of R_D and D considered in Figure 3, calculated according to eq 7, are τ_{mfp} = 67 ps (R_D = 10 nm, D = 10^{-3} cm^2 s^{-1}), 141 ps (R_D = 15 nm, D = 10^{-3} cm^2 s^{-1}), 667 ps (R_D = 10 nm, D = 10^{-4} cm^2 s^{-1}), and 1.5 ns (R_D = 15 nm, D = 10^{-4} cm^2 s^{-1}). Note that for all systems, τ_{mfp} is much larger than the charge separation time scale for excitons at the donor−acceptor interface (∼5 fs), estimated in Section 3. Thus, exciton diffusion is indeed the rate limiting process for exciton decay in this situation, and the assumption of instantaneous charge separation at the interface that is the physical basis for eq 3 is valid.

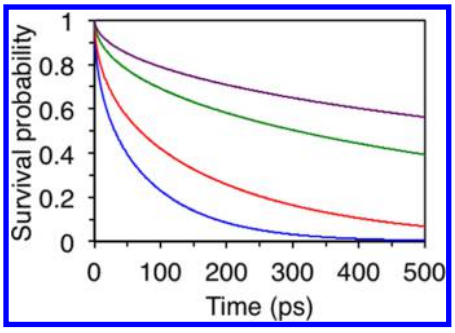

Figure 3. Survival probability for an exciton in a donor grain as a function of time for R_D = 10 nm and D = 10^{-3} cm^2 s^{-1} (blue), R_D = 15 nm and D = 10^{-3} cm^2 s^{-1} (red), R_D = 10 nm and D = 10^{-4} cm^2 s^{-1} (green), and R_D = 15 nm and D = 10^{-4} cm^2 s^{-1} (violet).

The value τ_{mfp} = 67 ps that is found for R_D = 10 nm and D = 10^{-3} cm^2 s^{-1} is comparable to the experimentally observed slower time scales of charge separation of ∼50 ps.[8] However, the calculations show that if R_D is increased or D is reduced relative to these values, the diffusion-controlled estimates significantly exceed the experimental values. This difference will be modified when exciton decay is taken into account, since this suppresses the contribution of long-lived exciton states and thereby shortens the overall charge separation time scales. Indeed, we note that even a small number of excitons reaching the donor−acceptor interface at very long times t significantly affects the mean first passage time. For instance, although τ_{mfp} = 1.5 ns for R_D = 15 nm and D = 10^{-4} cm^2 s^{-1}, this value reduces to 1.4, 1.0, and 0.41 ns (i.e., 140 fs), respectively, when only the excitons that arrive at the donor−acceptor interface within the

dx.doi.org/10.1021/jp508561z | J. Phys. Chem. C 2014, 118, 27235−27244

first 10, 5, and 2 ns, respectively, are considered. This is despite the fact that over 99% of all excitons dissociate within 10 ns, over 93% within 5 ns, and over 74% within 2 ns. This demonstrates that accounting for exciton decay would significantly suppress the contribution of long-lived excitons to the mean first passage time, and the time scale of diffusion-controlled exciton dissociation would then be expected to approach the experimental values.

5. DISCUSSION AND CONCLUSIONS

Recent experimental observations indicate that charge separation at the donor−acceptor interface of materials used in OPV cells takes place on at least two time scales following optical excitation, one of order ≤100 fs and the other of order ∼50−100 ps. These time scales have been interpreted as associated with coherent and diffusive time evolution of the exciton in the donor grain, respectively. In this paper we have analyzed these transport processes using available information on exciton delocalization/localization length, exciton diffusion coefficients, and system morphologies, in order to examine the consistency of this picture with the experimentally observed rates.

Our estimate of the fast time scale of exciton dissociation observed in BH−OPV systems was based on the assumption that this is dominated by the interfacial dissociation of excitons that are delocalized over several strongly interacting molecular sites such that (a) the dissociation rate is determined by the amplitude of the exciton wave function on interfacial sites and (b) the exciton delocalization rate (inverse of the intersite energy transfer coupling) is large enough (or conversely, that dephasing and dissipative effects are weak enough) to maintain delocalization during this short time scale. The dissociation rate of an exciton that starts on an interfacial site was estimated from the activationless limit of the Marcus theory to be of order 10^{-14} s^{-1}. Using available information on exciton delocalization length and donor grain sizes together with this simple estimate for excitonic dissociation enhanced by spatial coherence leads to charge separation rates of the observed order of magnitude. This description could in principle be extended to incorporate estimates of diffusive and/or superdiffusive contributions of dynamically propagating delocalized excitonic states, using e.g., the approach in ref 31 or more sophisticated dynamical calculations that explicitly incorporate excitonic coupling to phonon modes.[78−80] However, this current estimate already provides a clear indication that excitonic delocalization and the spatial coherence intrinsic to this can account for the observed fast time scale of charge separation in heterojunction photovoltaic systems.

For the diffusive ("long") time scale we have evaluated the mean first passage time (MPT) for an exciton localized on a molecular site to reach the grain boundary. We have argued that this provides a lower bound to the actual exciton lifetime if dissociation occurs only at the interface, but that this may be compensated by the possible contribution of longer range electron transfer (exciton dissociation from sites a little further than the interface). The rate evaluated from the inverse mean first passage time is consistent with the observed slow component of the charge separation process for smaller grain sizes ($R \approx 10$ nm) and larger diffusion coefficients ($D \approx 10^{-3}$ cm^2 s^{-1}), but becomes systematically somewhat smaller than experimentally measured values as the grain size increases and the diffusion coefficient decreases. We have shown that this can be explained by the fact that the inverse MPT of a diffusive process gives excessive weight to the contribution of slow dissociation events that occur on a time scale where exciton decay is already important. From the passage time distribution itself (Figure 3), we find that between 50% and 100% of the diffusion-controlled exciton dissociation is completed on time scales of the order of those observed experimentally.

It is useful to compare this picture of charge separation occurring on multiple time scales in bulk heterojunction photovoltaic cells with the corresponding situation in natural photosynthetic systems. In the latter, excitonic energy is transferred on time scales of fs−ps from antenna pigments to the reaction center where charge separation occurs to form membrane-stabilized charge separated states within ps−ns time scales.[81] While reaction centers can directly absorb light, it is typically chromophores in the antenna complexes that absorb the incident radiation. As discussed in Section 2, some extent of delocalization is common in the light harvesting antenna complexes, but since these are not in direct contact with the reaction center (more specifically, not directly coupled to the pigments responsible for charge separation, the so-called special pair P), there is no analogue of the ultrafast mechanism resulting from exciton delocalization over interfacial sites in the heterojunction photovoltaic systems. However, both excitonic delocalization and coherence play a significant role in the spatial transport of excitonic energy from the antenna to the reaction center, although they appear to have little effect on the overall efficiency or time scale of the energy transport (which is generally diffusive at long times as a result of energetic and dynamic disorder).[82] Since the time scale for charge separation within the reaction center is generally longer than that for excitonic energy transport from the antenna to the reaction center, unlike the situation in the heterojunction photovoltaic systems, the dynamics of charge separation in photosynthesis do not reflect the more subtle combination of coherent and incoherent dynamics seen for energy transport in BHJ-OPV cells that were discussed here.

In summary, we have made theoretical estimates of the rates expected for short time dissociation of spatially delocalized coherent excitonic states and a longer time diffusion-controlled dissociation of localized excitonic states for donor grain sizes 10−20 nm. Taken together with recent experimental observations of charge separation dynamics in bulk heterojunction photovoltaic systems, our results indicate that the kinetics of interfacial exciton dissociation in such systems is a multitime scale process that combines fast ($\tau \leq 100$ fs) dissociation of delocalized excitons and slow ($\tau \approx 50$−100 ps) diffusion-controlled dissociation. These times are predicted to be strongly morphology dependent. Further experiments should be able to verify this prediction.

■ ASSOCIATED CONTENT

Ⓢ Supporting Information

A detailed description of the techniques used for estimating the probability that the coherent exciton on the donor grain overlaps the interfacial region and for numerical evaluation of eqs 5 and 6. This material is available free of charge via the Internet at http://pubs.acs.org.

■ AUTHOR INFORMATION

Corresponding Author

*E-mail: whaley@berkeley.edu.

Notes

The authors declare no competing financial interest.

■ ACKNOWLEDGMENTS

K. B. W. thanks the Mortimer and Raymond Sackler Institute of Advanced Studies of Tel Aviv University for a visiting Sackler Lectureship in 2013 during which this work was initiated. The research of K.B.W. is supported and by DARPA under award N66001-10-1-4068. A.A.K. acknowledges the financial support of The Netherlands Organization for Scientific Research (NWO) Rubicon grant No. 680-50-1022. The research of A.N. is supported by the Israel Science Foundation and the Israel-US Binational Science Foundation (grant no. 2011509). K. B. W. is a member of the Kavli Energy NanoSciences Institute at the University of California, Berkeley and the Lawrence Berkeley National Laboratory. We thank Mark Ratner, Brett Savoie, and Zeev Schuss for very helpful discussions.

■ REFERENCES

(1) Mikhnenko, O. V.; Lin, J.; Shu, Y.; Anthony, J. E.; Blom, P. W. M.; Nguyen, T.-Q.; Loi, M. A. Effect of Thermal Annealing on Exciton Diffusion in a Diketopyrrolopyrrole Derivative. *Phys. Chem. Chem. Phys.* **2012**, *14*, 14196−14201.

(2) Menke, S. M.; Luhman, W. A.; Holmes, R. J. Tailored Exciton Diffusion in Organic Photovoltaic Cells for Enhanced Power Conversion Efficiency. *Nat. Mater.* **2013**, *12*, 152−157.

(3) Hoppe, H.; Niggemann, M.; Winder, C.; Kraut, J.; Hiesgen, R.; Hinsch, A.; Meissner, D.; Sariciftci, N. S. Nanoscale Morphology of Conjugated Polymer/Fullerene-Based Bulk-Heterojunction Solar Cells. *Adv. Funct. Mater.* **2004**, *14*, 1005−1011.

(4) Ma, W.; Gopinathan, A.; Heeger, A. J. Nanostructure of the Interpenetrating Networks in Poly(3-Hexylthiophene)/Fullerene Bulk Heterojunction Materials: Implications for Charge Transport. *Adv. Mater.* **2007**, *19*, 3656−3659.

(5) Moon, J. S.; Takacs, C. J.; Cho, S.; Coffin, R. C.; Kim, H.; Bazan, G. C.; Heeger, A. J. Effect of Processing Additive on the Nanomorphology of a Bulk Heterojunction Material. *Nano Lett.* **2010**, *10*, 4005−4008.

(6) Gu, Y.; Wang, C.; Russell, T. P. Multi-Length-Scale Morphologies in PCPDTBT/PCBM Bulk-Heterojunction Solar Cells. *Adv. Energy Mater.* **2012**, *2*, 683−690.

(7) Jailaubekov, A. E.; Willard, A. P.; Tritsch, J. R.; Chan, W.-L.; Sai, N.; Gearba, R.; Kaake, L. G.; Williams, K. J.; Leung, K.; Rossky, P. J.; Zhu, X. Y. Hot Charge-Transfer Excitons Set the Time Limit for Charge Separation at Donor/Acceptor Interfaces in Organic Photovoltaics. *Nat. Mater.* **2013**, *12*, 66−73.

(8) Kaake, L. G.; Moses, D.; Heeger, A. J. Coherence and Uncertainty in Nanostructured Organic Photovoltaics. *J. Phys. Chem. Lett.* **2013**, *4*, 2264−2268.

(9) Guo, J.; Ohkita, H.; Benten, H.; Ito, S. Charge Generation and Recombination Dynamics in Poly(3-Hexylthiophene)/Fullerene Blend Films with Different Regioregularities and Morphologies. *J. Am. Chem. Soc.* **2010**, *132*, 6154−6164.

(10) Marsh, R. A.; Hodgkiss, J. M.; Albert-Seifried, S.; Friend, R. H. Effect of Annealing on P3HT:PCBM Charge Transfer and Nanoscale Morphology Probed by Ultrafast Spectroscopy. *Nano Lett.* **2010**, *10*, 923−930.

(11) Grancini, G.; Maiuri, M.; Fazzi, D.; Petrozza, A.; Egelhaaf, H. J.; Brida, D.; Cerullo, G.; Lanzani, G. Hot Exciton Dissociation in Polymer Solar Cells. *Nat. Mater.* **2013**, *12*, 29−33.

(12) Spencer, S.; Cody, J.; Misture, S.; Cona, B.; Heaphy, P.; Rumbles, G.; Andersen, J.; Collison, C. Critical Electron Transfer Rates for Exciton Dissociation Governed by Extent of Crystallinity in Small Molecule Organic Photovoltaics. *J. Phys. Chem. C* **2014**, *118*, 14840−14847.

(13) Markov, D. E.; Tanase, C.; Blom, P. W. M.; Wildeman, J. Simultaneous Enhancement of Charge Transport and Exciton Diffusion in Poly(*p*-Phenylene Vinylene) Derivatives. *Phys. Rev. B* **2005**, *72*, 045217.

(14) Huang, Y.; Kramer, E. J.; Heeger, A. J.; Bazan, G. C. Bulk Heterojunction Solar Cells: Morphology and Performance Relationships. *Chem. Rev.* **2014**, *114*, 7006−7043.

(15) Heitzer, H. M.; Savoie, B. M.; Marks, T. J.; Ratner, M. A. Organic Photovoltaics: Elucidating the Ultra-Fast Exciton Dissociation Mechanism in Disordered Materials. *Angew. Chem., Int. Ed.* **2014**, *53*, 1−6.

(16) Wang, H.; Wang, H.-Y.; Gao, B.-R.; Wang, L.; Yang, Z.-Y.; Du, X.-B.; Chen, Q.-D.; Song, J.-F.; Sun, H.-B. Exciton Diffusion and Charge Transfer Dynamics in Nano Phase-Separated P3HT/PCBM Blend Films. *Nanoscale* **2011**, *3*, 2280−2285.

(17) Fast charge separation can also indicate impure phases, i.e., an incomplete separation between the donor and acceptor regions.[15] However, it is hard to accommodate such a picture with the observed large difference between the slow and the fast charge separation time scales described above.

(18) Dubin, F.; Melet, R.; Barisien, T.; Grousson, R.; Legrand, L.; Schott, M.; Voliotis, V. Macroscopic Coherence of a Single Exciton State in an Organic Quantum Wire. *Nat. Phys.* **2006**, *2*, 32−35.

(19) Mukamel, S. Comment on "Coherence and Uncertainty in Nanostructured Organic Photovoltaics". *J. Phys. Chem. A* **2013**, *117*, 10563−10564.

(20) Zhang, W. M.; Meier, T.; Chernyak, V.; Mukamel, S. Exciton-Migration and Three-Pulse Femtosecond Optical Spectroscopies of Photosynthetic Antenna Complexes. *J. Chem. Phys.* **1998**, *108*, 7763−7774.

(21) Wang, T.; Chan, W.-L. Dynamical Localization Limiting the Coherent Transport Range of Excitons in Organic Crystals. *J. Phys. Chem. Lett.* **2014**, *5*, 1812−1818.

(22) Chan, W.-L.; Ligges, M.; Jailaubekov, A.; Kaake, L.; Miaja-Avila, L.; Zhu, X.-Y. Observing the Multiexciton State in Singlet Fission and Ensuing Ultrafast Multielectron Transfer. *Science* **2011**, *334*, 1541−1545.

(23) Chan, W.-L.; Berkelbach, T. C.; Provorse, M. R.; Monahan, N. R.; Tritsch, J. R.; Hybertsen, M. S.; Reichman, D. R.; Gao, J.; Zhu, X. Y. The Quantum Coherent Mechanism for Singlet Fission: Experiment and Theory. *Acc. Chem. Res.* **2013**, *46*, 1321−1329.

(24) The external quantum efficiency is defined as the ratio between the number of electrons flowing out of a device and the number of photons incident on it. The internal quantum efficiency is defined as the number of electrons collected per photon absorbed.

(25) The yield also decreases for $d > 15$ nm, reflecting the finite triplet lifetime.

(26) Wilson, M. W. B.; Rao, A.; Clark, J.; Kumar, R. S. S.; Brida, D.; Cerullo, G.; Friend, R. H. Ultrafast Dynamics of Exciton Fission in Polycrystalline Pentacene. *J. Am. Chem. Soc.* **2011**, *133*, 11830−11833.

(27) Chan, W.-L.; Ligges, M.; Zhu, X. Y. The Energy Barrier in Singlet Fission Can Be Overcome through Coherent Coupling and Entropic Gain. *Nat. Chem.* **2012**, *4*, 840−845.

(28) Hwang, I.; Scholes, G. D. Electronic Energy Transfer and Quantum-Coherence in Π-Conjugated Polymers. *Chem. Mater.* **2010**, *23*, 610−620.

(29) In natural light harvesting systems, it is possible to also generate excitonic coherences and hence superpositions of excitonic states from an initial single excitonic state, due to the non-Markovian behavior of the nuclear dynamics.[30]

(30) Fassioli, F.; Olaya-Castro, A.; Scholes, G. D. Coherent Energy Transfer under Incoherent Light Conditions. *J. Phys. Chem. Lett.* **2012**, *3*, 3136−42.

(31) Moix, J. M.; Khasin, M.; Cao, J. Coherent Quantum Transport in Disordered Systems: I. The Influence of Dephasing on the Transport Properties and Absorption Spectra on One-Dimensional Systems. *New J. Phys.* **2013**, *15*, 085010.

(32) Guo, J.; Ohkita, H.; Benten, H.; Ito, S. Near-IR Femtosecond Transient Absorption Spectroscopy of Ultrafast Polaron and Triplet Exciton Formation in Polythiophene Films with Different Regioregularities. *J. Am. Chem. Soc.* **2009**, *131*, 16869−16880.

(33) Meier, T.; Chernyak, V.; Mukamel, S. Multiple Exciton Coherence Sizes in Photosynthetic Antenna Complexes Viewed by Pump−Probe Spectroscopy. *J. Phys. Chem. B* **1997**, *101*, 7332−7342.
(34) Singh, J.; Bittner, E. R.; Beljonne, D.; Scholes, G. D. Fluorescence Depolarization in Poly[2-Methoxy-5-((2-Ethylhexyl)-Oxy)-1,4-Phenylenevinylene]: Sites Versus Eigenstates Hopping. *J. Chem. Phys.* **2009**, *131*, 194905.
(35) Knoester, J. Modeling the Optical Properties of Excitons in Linear and Tubular J-Aggregates. *Int. J. Photoenergy* **2006**, *2006*, 61364.
(36) Bakalis, L. D.; Knoester, J. Pump−Probe Spectroscopy and the Exciton Delocalization Length in Molecular Aggregates. *J. Phys. Chem. B* **1999**, *103*, 6620−6628.
(37) Dijkstra, A. G.; la Cour Jansen, T.; Knoester, J. Localization and Coherent Dynamics of Excitons in the Two-Dimensional Optical Spectrum of Molecular J-Aggregates. *J. Chem. Phys.* **2008**, *128*, 164511.
(38) Tempelaar, R.; Spano, F. C.; Knoester, J.; Jansen, T. L. C. Mapping the Evolution of Spatial Exciton Coherence through Time-Resolved Fluorescence. *J. Phys. Chem. Lett.* **2014**, *5*, 1505−1510.
(39) Würthner, F.; Kaiser, T. E.; Saha-Möller, C. R. J-Aggregates: From Serendipitous Discovery to Supramolecular Engineering of Functional Dye Materials. *Angew. Chem., Int. Ed.* **2011**, *50*, 3376−3410.
(40) van Burgel, M.; Wiersma, D. A.; Duppen, K. The Dynamics of One-Dimensional Excitons in Liquids. *J. Chem. Phys.* **1995**, *102*, 20−33.
(41) Heiber, M. C.; Dhinojwala, A. Estimating the Magnitude of Exciton Delocalization in Regioregular P3HT. *J. Phys. Chem. C* **2013**, *117*, 21627−21634.
(42) Peierls, R. E. *Quantum Theory of Solids*; Oxford University Press: Oxford, UK, 1964; p 108.
(43) Hagler, T. W.; Pakbaz, K.; Voss, K. F.; Heeger, A. J. Enhanced Order and Electronic Delocalization in Conjugated Polymers Oriented by Gel Processing in Polyethylene. *Phys. Rev. B* **1991**, *44*, 8652−8666.
(44) Ritz, T.; Park, S.; Schulten, K. Kinetics of Excitation Migration and Trapping in the Photosynthetic Unit of Purple Bacteria. *J. Phys. Chem. B* **2001**, *105*, 8259−8267.
(45) Yang, M.; Damjanović, A.; Vaswani, H. M.; Fleming, G. R. Energy Transfer in Photosystem I of Cyanobacteria Synechococcus Elongatus: Model Study with Structure-Based Semi-Empirical Hamiltonian and Experimental Spectral Density. *Biophys. J.* **2003**, *85*, 140−158.
(46) Bennett, D. I. G.; Amarnath, K.; Fleming, G. R. A Structure-Based Model of Energy Transfer Reveals the Principles of Light Harvesting in Photosystem II Supercomplexes. *J. Am. Chem. Soc.* **2013**, *135*, 9164−9173.
(47) The antenna complex of green sulfur bacteria is an interesting exception, containing no protein and consisting only of highly organized structures − chlorosomes − containing ∼250 000 chlorophyll molecules, resulting in highly effective light harvesting at even the lowest light intensities.
(48) Herek, J. L.; Fraser, N. J.; Pullerits, T.; Martinsson, P.; Polívka, T.; Scheer, H.; Cogdell, R. J.; Sundström, V. B800→B850 Energy Transfer Mechanism in Bacterial LH2 Complexes Investigated by B800 Pigment Exchange. *Biophys. J.* **2000**, *78*, 2590−2596.
(49) van Grondelle, R.; Novoderezhkin, V. Dynamics of Excitation Energy Transfer in the LH1 and LH2 Light-Harvesting Complexes of Photosynthetic Bacteria. *Biochemistry* **2001**, *40*, 15057−15068.
(50) Collini, E.; Wong, C. Y.; Wilk, K. E.; Curmi, P. M. G.; Brumer, P.; Scholes, G. D. Coherently Wired Light-Harvesting in Photosynthetic Marine Algae at Ambient Temperature. *Nature* **2010**, *463*, 644−647.
(51) Brixner, T.; Stenger, J.; Vaswani, H. M.; Cho, M.; Blankenship, R. E.; Fleming, G. R. Two-Dimensional Spectroscopy of Electronic Couplings in Photosynthesis. *Nature* **2005**, *434*, 625−628.
(52) Jang, S.; Newton, M. D.; Silbey, R. J. Multichromophoric Förster Resonance Energy Transfer. *Phys. Rev. Lett.* **2004**, *92*, 218301.
(53) Novoderezhkin, V. I.; van Grondelle, R. Physical Origins and Models of Energy Transfer in Photosynthetic Light-Harvesting. *Phys. Chem. Chem. Phys.* **2010**, *12*, 7352−7365.
(54) Scholes, G. D. Long-Range Resonance Energy Transfer in Molecular Systems. *Annu. Rev. Phys. Chem.* **2003**, *54*, 57−87.
(55) Seth, L.; Masoud, M. Symmetry-Enhanced Supertransfer of Delocalized Quantum States. *New J. Phys.* **2010**, *12*, 075020.
(56) Hoyer, S.; Ishizaki, A.; Whaley, K. B. Spatial Propagation of Excitonic Coherence Enables Ratcheted Energy Transfer. *Phys. Rev. E* **2012**, *86*, 041911.
(57) Jang, S.; Hoyer, S.; Fleming, G.; Whaley, K. B. Generalized Master Equation for Modular Exciton Density Transfer. *Phys. Rev. Lett.* **2014**, *113*, 188102.
(58) Jang, S.; Newton, M. D.; Silbey, R. J. Multichromophoric Förster Resonance Energy Transfer from B800 to B850 in the Light Harvesting Complex 2: Evidence for Subtle Energetic Optimization by Purple Bacteria. *J. Phys. Chem. B* **2007**, *111*, 6807−6814.
(59) It should be noted that excitonic delocalization, which yields coherence within a site basis description, represents only one aspect of the quantum coherence that plays a role in energy transport in these systems. Recent time-resolved experiments with femtosecond lasers have revealed excitonic coherences following broad band excitation.[60]
(60) Engel, G. S.; Calhoun, T. R.; Read, E. L.; Ahn, T.-K.; Mancal, T.; Cheng, Y.-C.; Blankenship, R. E.; Fleming, G. R. Evidence for Wavelike Energy Transfer through Quantum Coherence in Photosynthetic Systems. *Nature* **2007**, *446*, 782−786.
(61) Shabani, A.; Mohseni, M.; Rabitz, H.; Lloyd, S. Efficient Estimation of Energy Transfer Efficiency in Light-Harvesting Complexes. *Phys. Rev. E* **2012**, *86*, 011915.
(62) Hoyer, S.; Sarovar, M.; Whaley, K. B. Limits of Quantum Speedup in Photosynthetic Light Harvesting. *New J. Phys.* **2010**, *12*, 065041.
(63) Haken, H.; Strobl, G. An Exactly Solvable Model for Coherent and Incoherent Exciton Motion. *Z. Phys.* **1973**, *262*, 135−148.
(64) Caruso, F.; Chin, A. W.; Datta, A.; Huelga, S. F.; Plenio, M. B. Highly Efficient Energy Excitation Transfer in Light-Harvesting Complexes: The Fundamental Role of Noise-Assisted Transport. *J. Chem. Phys.* **2009**, *131*, 105106.
(65) Rebentrost, P.; Mohseni, M.; Kassal, I.; Lloyd, S.; Aspuru-Guzik, A. Environment-Assisted Quantum Transport. *New J. Phys.* **2009**, *11*, 033003.
(66) Bittner, E. R.; Silva, C. Noise-Induced Quantum Coherence Drives Photo-Carrier Generation Dynamics at Polymeric Semiconductor Heterojunctions. *Nat. Commun.* **2014**, *5*, 3119.
(67) Paraecattil, A. A.; Banerji, N. Charge Separation Pathways in a Highly Efficient Polymer: Fullerene Solar Cell Material. *J. Am. Chem. Soc.* **2014**, *136*, 1472−1482.
(68) Scholes, G. D.; Smyth, C. Perspective: Detecting and Measuring Exciton Delocalization in Photosynthetic Light Harvesting. *J. Chem. Phys.* **2014**, *140*, 110901.
(69) Congreve, D. N.; Lee, J.; Thompson, N. J.; Hontz, E.; Yost, S. R.; Reusswig, P. D.; Bahlke, M. E.; Reineke, S.; Van Voorhis, T.; Baldo, M. A. External Quantum Efficiency above 100% in a Singlet-Exciton-Fission-Based Organic Photovoltaic Cell. *Science* **2013**, *340*, 334−337.
(70) Gélinas, S.; Rao, A.; Kumar, A.; Smith, S. L.; Chin, A. W.; Clark, J.; van der Poll, T. S.; Bazan, G. C.; Friend, R. H. Ultrafast Long-Range Charge Separation in Organic Semiconductor Photovoltaic Diodes. *Science* **2014**, *343*, 512−516.
(71) Provencher, F.; Bérubé, N.; Parker, A. W.; Greetham, G. M.; Towrie, M.; Hellmann, C.; Côté, M.; Stingelin, N.; Silva, C.; Hayes, S. C. Direct Observation of Ultrafast Long-Range Charge Separation at Polymer−Fullerene Heterojunctions. *Nat. Commun.* **2014**, *5*, 4288.
(72) We disregard such coupling in all but interface sites, since energetic considerations allow exciton dissociation only at the interface.
(73) Nitzan, A. *Chemical Dynamics in Condensed Phases*; Oxford University Press: Oxford, UK, 2006.
(74) Nagasawa, Y.; Yartsev, A. P.; Tominaga, K.; Johnson, A. E.; Yoshihara, K. Temperature Dependence of Ultrafast Intermolecular Electron Transfer Faster Than Solvation Process. *J. Chem. Phys.* **1994**, *101*, 5717−5726.

(75) Gilch, P.; Zinth, E. B.; Stockl, M.; Harter, P.; Feilitzsch, T. v.; Miche-Beyerle, M. E. In *The Thirteenth International Conference on Ultrafast Phenomena*; Optical Society of America: Vancouver, Canada, 2002; p ME17.
(76) Huber, R.; Moser, J.-E.; Grätzel, M.; Wachtveitl, J. Real-Time Observation of Photoinduced Adiabatic Electron Transfer in Strongly Coupled Dye/Semiconductor Colloidal Systems with a 6 fs Time Constant. *J. Phys. Chem. B* **2002**, *106*, 6494−6499.
(77) Polking, J.; Boggess, A.; Arnold, D. *Differential Equations with Boundary Value Problems*, 2nd ed.; Pearson: Upper Saddle River, NJ, 2005.
(78) Cheng, Y.-C.; Fleming, G. R. Dynamics of Light Harvesting in Photosynthesis. *Annu. Rev. Phys. Chem.* **2009**, *60*, 241−262.
(79) Ishizaki, A.; Fleming, G. R. Unified Treatment of Quantum Coherent and Incoherent Hopping Dynamics in Electronic Energy Transfer: Reduced Hierarchy Equation Approach. *J. Chem. Phys.* **2009**, *130*, 234111.
(80) Ishizaki, A.; Calhoun, T. R.; Schlau-Cohen, G. S.; Fleming, G. R. Quantum Coherence and Its Interplay with Protein Environments in Photosynthetic Electronic Energy Transfer. *Phys. Chem. Chem. Phys.* **2010**, *12*, 7319−7337.
(81) Hillier, W.; Babcock, G. T. Photosynthetic Reaction Centers. *Plant Physiology* **2001**, *125*, 33.
(82) See, e.g.: Jesenko, S.; Žnidarič, M. Excitation Energy Transfer Efficiency: Equivalence of Transient and Stationary Setting and the Absence of Non-Markovian Effects. *J. Chem. Phys.* **2013**, *138*, 174103.